Astronomy & Astrophysics manuscript no. clash˙photoz˙v0
May 7, 2012

CLASH: Photometric redshifts with 16 HST bands for galaxy clusters

S. Jouvel[1,2] and the CLASH team

[1] University College London, Gower street, London WC1E 6BT, UK
[2] Institut de Cincies de l'Espai (IEEC-CSIC), E-08193 Bellaterra (Barcelona), Spain
[3] Space Telescope Science Institute, 3700 San Martin Drive, Baltimore, MD 21218, USA
[4] Granada
[5] Munich

DRAFT VERSION: MAY 7, 2012

ABSTRACT

Context. The CLASH survey is an HST multi-cycle treasury program (Postman et al. 2010) whose main focus is at deriving galaxy clusters mass concentration based on the strong lensing effect for 25 massive clusters. CLASH uses galaxy colors from 16 HST bands photometry to derive reliable estimates of galaxy distances using photometric redshifts methods.
Aims. In this paper, we study the CLASH photometric redshift estimation. We aim at demonstrate that photometric redshift techniques reach an accuracy that enables their use in dark matter mass models estimation from the strong-lensing analysis.
Methods. We use Le Phare and BPZ photometric redshift codes which are publicly available. Both are based on template fitting methods but have differences in their procedure allowing interesting comparisons. We use all clusters photometry available up to date to give a first estimation of the photoz accuracy for the CLASH data. We then focus on the MACS1206 cluster to study the photoz accuracy of the multiple images which have spectroscopic redshifts.
Results. We reach an accuracy of 2%(1+z) when pruning from the bad fits and 4%(1+z) without any selection. We propagate this redshift error into a distance measurement error and show that photometric redshifts from CLASH are reliable enough to allow their use in the mass model reconstruction. Using catalogues simulation, we show that this accuracy is the best we can achieve with the CLASH photometry when taking into account extinction from dust, emission lines and template representativity. We also describe and release a photometric redshift catalogue of MACS1206.
Conclusions. We show that photometric redshifts are accurate enough to enable their use in the mass model reconstruction from strong lensing analysis. We also show the limit of broad-band photometry in terms of photometric redshift accuracy.

Key words. CLASH – Photometric Redshift – Lensing Surveys – Dark Energy – Cosmology

1. Introduction

Using 16 photometric bands onboard the HST, the CLASH program (Postman et al. 2012) studies massive galaxy clusters. The high mass-density of these clusters produces strong and weak lensing features. Through a study of both the strong and weak-lensing effect, one can look at the cluster mass, structure and sub-structure which help understanding dark matter spatial repartition and structure formation scenario. One of the primary goal of CLASH is to focus on the mass-concentration relation derived using strong lensing models of those clusters. When considering the lensing effect, we divide galaxies in 3 kinds : 1- the foreground galaxies, 2- the cluster members and 3- background galaxies. Foreground galaxies are located between the cluster and our galaxy along the line of sight. The cluster member are the galaxies of the clusters that are producing the lensing signal along with their dark matter haloes. Background galaxies are located behind the galaxy cluster, along the line of sight. In analysing the shape of bakgroung galaxies, we extract the lensing signal. For the strong-lensing analysis, we are interested in the multiply imaged and strongly elongated galaxies close to the cluster center. In studying the position of the mutiple images, one can derive the cluster mass and matter distribution enclosed inside the strong-lensing region. However, one needs to have an estimate of the multiple images distances to derive the cluster magnification.

The CLASH program uses galaxy colors based on current photometric redshifts (hereafter photoz) techniques to estimate galaxy distances with a great precision. The photoz are ultimately used to dissociate the foreground/background and cluster member in the field. The utilisation of photoz in the strong lensing field is a particularity of the CLASH strategy. Indeed, strong-lensing analysis prefers to use spectroscopic redshifts (hereafter specz) to obtain the redshift of the arcs candidates. However, the recent progress of the photoz field combined with the excellent photometry in the large number of bands available in the CLASH survey makes photoz more accurate and useful for the strong lensing analysis. Photoz have the advantages to give a redshift estimation at any depth for all the galaxies in the field which is not possible with current spectroscopic redshift techniques. Arcs are often faint objects and difficult to reach with ground based telescopes. Photoz are then a definite asset to assess the redshift of the multiple images to be used in the lensing modelling.

In this paper, we first focus on the photometric redshift of all galaxies of several clusters observed by CLASH. In section 2, we give a quick overview of the scientific goals of the CLASH program for which the photometric redshift play an important role. We then describe the CLASH photometry in section **??**. Section 3 presents the 2 photometric redshift techniques we use in this paper along with a first assessment on their reliability in the case of CLASH photometry. Using all spectroscopic red-

Send offprint requests to: Stéphanie Jouvel, e-mail: s.jouvel@ucl.ac.uk

shifts available for the CLASH data, we study the photometric redshift accuracy in section 4 for the galaxy clusters and the multiple images systems of all clusters. In section 4.2, we use mock galaxy catalogues from Jouvel et al. (2009) to have a better understanding of the systematics from galaxy properties on the photoz results. This section shows the limitation of broad-band photometry in the photoz estimation. We then give a first estimation of the impact of the photoz accuracy on the mass reconstruction from strong lensing analysis in section 6. We then focus on MACS1206 cluster in section 5 in order to study the photometric redshift of the multiple images systems in greater details. In the last section 7, we describe the photoz catalogue we have produced for the MACS1206 field. Throughout this paper we assume a flat Lambda-CDM cosmology and use the AB magnitude system.

2. The CLASH program

The CLASH -Cluster Lensing And Supernova with Hubble- is an ongoing HST multicycle treasury program (Postman et al. 2012). It targets massive galaxy clusters selected to have smoothed relaxed X-ray profiles. It primarily aims at studying the mass-concentration relation, dark matter content, galaxy properties but also finding high-redshift galaxies using the lensing effect. The main motivation for this survey is to test the Λ CDM scenario. The final cluster sample will contain observations of 25 of the most massive clusters known today observed in 16 broad bands covering from UV to NIR wavelengths. The cluster selection and survey strategy is described in Postman et al. (2012).

2.1. CLASH science and photometric redshifts

2.1.1. Weak lensing mass reconstruction

WL mass reconstructions require that the mean redshift of background galaxies (at every spatial resolution element) are not biased. Since the Dds/Ds distance ratio of deflector-source (Dds) and observer-source (Ds) rises steeply behind the cluster, and then flattens off, it is most important to have no photoz bias in the steep part of the Dds/Ds. Figure 8 shows the relative error on the Dds/Ds ratio as a function of the source redshift for different deflector redshifts assuming a photoz error of 0.02(1+z). The example shows that for a cluster at z=0.5 and sources at redshifts higher than 3 the fractional error in Dds/Ds becomes the same if the source is missplaced from z=3 and to z=4. We will study this in more detail in section 6.

The lensing mass converence is usually estimated from the shear signal assuming the mean background redshift to be known. This mean redshift can be biased because many galaxies are slightly displaced, i.e. the photometric redshift estimate is 0.9 or 1.1 instead of 1.0, or because most galaxies are correctly placed but a few outliers which are at rather low or rather high redshift enter the sample. For fields with a cluster in the foreground special attention has to be payed to measure the fraction of cluster members beeing missplaced at high redshift and thus entering the weak lensing 'background' sample. With the many filters placed on the blue and red part around the 4000A break of the cluster members, this fraction will be low in the CLASH sample as we show in section 4.

2.1.2. Strong lensing mass reconstruction

Strong Lensing analyses use the photometric redshift estimates of individual galaxies in the lens modelling. Catastropic outliers with very differrent redshifts play a minor role, since the low redshift hypothesis can usually be ruled out because galaxies would not be strongly lensed then anymore, or because they contradict the model variety still allowed from the few spectroscopic redshifts usually available for every cluster (giant arcs etc.). Slightly wrong redshifts (δz=0.2) can have a significant impact, they can lead to a model-tension because positions can not be correctly reproduced simulataneously (even if the model is correct). If a mass distribution is constrained by many multiple images, wrong photometric redshift estimates can also be identified for individual objects. There is however also the possibility that a wrong concentration is inferred. This can be understood if one considers sources at different redshift that are mapped to einstein radii of different size. If there is a bias that is a monotonic function of redshift, then a model with wrong concentration will be found to be a good model.

Another issue is that the photometry of multiple images and arcs is usually affected by systematic errors at a higher degree. Hence, one should investigate the photoz accuracy for objects with high cluster light contamination seperately. We study the photometric redshift for the arcs in section 5. The impact of the photometric redshift accuracy on the strong lensing mass reconstruction is studied in 6.

2.1.3. Cluster membership

The assignement for cluster membership plays a role in parametrized SL analyses (where the mass traced by member is explicitely modelled), but also in non parameteric models where the smooth cluster light distribution is somehow included in the modeling. Therefore one would like to get membership right. Also, if one wants to correlate the obtained WL/SL mass maps with the positions of cluster members to investigate in which kind of (line-of-sight projected) environment galaxies 'live' one would like to have a sample that is complete with low contamination.

On the other hand, the latter kind of investigations are tricky because one never knows even from ultimately precise photometric redshifts whether a galaxy is in the cluster or just associated to the LSS around the cluster (filaments, further groups along the LOS which is associated to the cluster but not in the cluster). If one would like to study galaxy transformation in enhanced DM density environments, one would probably use spectroscopic data.

2.2. The CLASH photometry

We have completed observations for 12 clusters in the 16 HST bands using the WFC3 NIR and UVIS channel and the ACS camera. The photometry is a critical issue in photometric redshift accuracy. It is especially critical for the faint galaxies and the arcs that often have elongated shapes. We detail below the photometric quality and completness of the CLASH data for the online catalogues. However the arcs photometry is computed following a different procedure that we will explain in section 5.

The photometry is measured in isophotal apertures and corrected for both galactic extinction using Schlegel et al. (1998) and finite aperture size. Flux uncertainties are taken directly from SExtractor Bertin & Arnouts (1996). We find consistency

comparing our observed flux uncertainties with those predicted from the ETCs (HST exposure time calculators). The background light is subtracted by SExtractor for detection setting SExtractor parameters to:

– BACK_SIZE 64
– BACK_FILTERSIZE 3
(estimated in a 3x3 grid of boxes, each 64x64 pixels)

To photometry we use :

– BACKPHOTO_TYPE LOCAL
– BACKPHOTO_THICK 26
(estimated individually for each object within in a rectangular annulus of thickness of 26 pixels drawn around that object)

We do not model and substract cluster galaxies and background light in this paper. It is a potential contaminent in the photometry and will likely induce biases in the photometric redshift results. SExtractor models the background locally but the arcs are potentially faint and have complex shapes. The best photometry will be performed using models of the background and cluster galaxies in a more accurate way using methods such as wavelets reconstruction. This will be investigated in an other paper Jouvel et al. (2010). In this paper, we will analyse only SExtractor and colorPro Coe et al. (2006) output photometry.

The detection images are weighted sums of images in individual filters. In this paper, we use a combination of all IR filters for the source detection. Concerning the detection parameters, we systematically explore a range of possible values. The cluster environement makes it difficult to arrive at an ideal setup for all galaxies. For example, the 3x3 grid of 64x64 pixel boxes is too small for some of the BCGs which can span almost ≈1,000 pixels (≈1 arcmin) from north to south in the IR. We thus use :

– DETECT_MINAREA 5
– DETECT_THRESH 2.5
– ANALYSIS_THRESH 1.5
– DEBLEND_MINCONT 0.0001
– DEBLEND_NTHRESH 64
– CLEAN Y
– CLEAN_PARAM 1.2

Table 1 is a list of the camera and filters used for the CLASH observations with their 5σ depth and the percentage of galaxies detected for each filter at F814<26 AB mag. The magnitude limits shown are calculated on all galaxies without regards of their sizes. A more standard definition of depth is found in Postman et al. (2012). The bluest bands have a deficit of galaxies due to the drop of the HST system transmission (mirror-optics-filters). For example F225W reach an efficiency of 10% at the peak wavelength. The efficiency increase for F390W and reach an efficiency of 25% at the peak wavelength. Compared to F814W, the number of photons will be about 4 times less. The CLASH survey strategy is to spend more time observing in the bluest band in order to compensate the efficiency loss.

Table 1. List of observations by bands, magnitude limit at 5σ and completeness. These magnitudes limit are an average over galaxies of different sizes as we need this for the simulation.

Camera	# Filter	AB mag (5σ)	% i<26
WFC3/UVIS	F225W	23.9	69.0
WFC3/UVIS	F275W	24.3	69.5
WFC3/UVIS	F336W	24.8	78.3
WFC3/UVIS	F390W	25.9	91.7
ACS/WFC	F435W	26.1	94.3
ACS/WFC	F475W	26.5	97.9
ACS/WFC	F606W	27.2	98.4
ACS/WFC	F625W	26.6	99.4
ACS/WFC	F775W	26.6	99.5
ACS/WFC	F814W	27.3	99.4
ACS/WFC	F850LP	26.3	99.4
WFC3/IR	F105W	27.1	99.2
WFC3/IR	F110W	27.7	85.3
WFC3/IR	F125W	27.1	87.1
WFC3/IR	F140W	27.2	94.9
WFC3/IR	F160W	27.2	97.7

3. Photometric redshifts estimation

Most of the spectroscopic redshifts sample are cluster members at $z < 0.8$ and spans a magnitude range between 18<F814<25 as shown in Figure 1. We gathered spectroscopic redshifts from litterature but most of specz have been targetted by the VLT/VIMOS Large Programme 186.A-0798 as detailed in Table A.1. Using galaxies at $z < 1$, we study the photometric redshift accuracy and compare photoz results from both Le Phare and BPZ code in section 4. We also study the photometric redshift accuracy of the multiple images for all the CLASH clusters up to date in section 5.

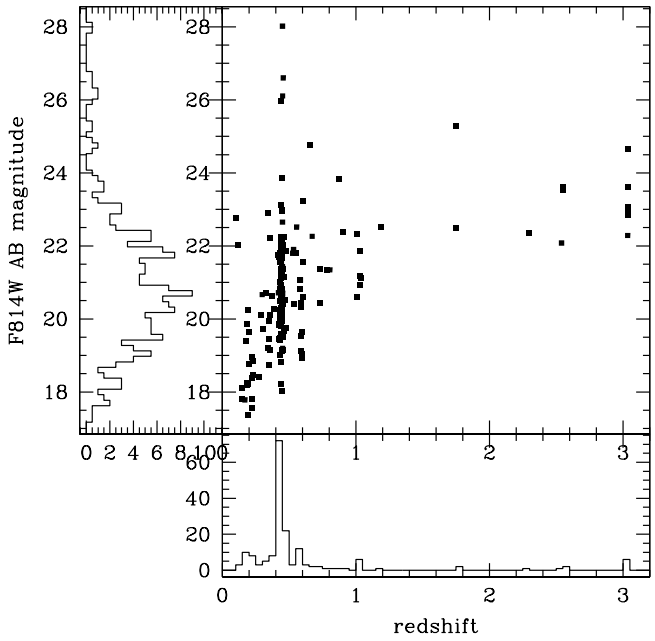

Fig. 1. Magnitude F814W as a function of redshift for the spectroscopic redshifts gathered for all CLASH clusters up to date.

There is different photoz techniques such as Neural Network Collister & Lahav (2004); Vanzella et al. (2004), template fitting Benítez (2000); Ilbert et al. (2006), decision trees Cunha et al. (2011) and polynomial fits. From all the methods available, only template fitting ones can be used with our spectroscopic redshift sample. Indeed methods that require training sets are sensitive to colors-magnitude-redshift relations so one need a representative training set that samples the whole photometric survey which we do not have here. Our spectroscopic redshift sample is likely to be biased towards red galaxies since the galaxies for which we

have a specz are mainly cluster members as shown in 1 and the redshift distribution is very sparse since peaked at clusters redshifts. In this paper we use BPZ and Le Phare. Below we give a quick description these methods. An estimation of performances on simulations and real data for BPZ and Le Phare can be found in Hildebrandt et al. (2010).

3.1. Le Phare

Le Phare[1] is a public photometric redshift code based on a template fitting method used in Ilbert et al. (2006, 2009). It uses a χ^2 minimisation defined as :

$$\chi^2_{model} = \sum_{i=1}^{n} ([F^i_{obs} - \alpha F^i_{model}]/\sigma^i)^2 \quad (1)$$

where F^i_{obs} and F^i_{model} are the observed and the template model fluxes inside a filter i and σ^i is the photometric error for this filter. For the model library we use the templates optimised for the COSMOS photometric redshift described in Ilbert et al. (2009). The library is composed by 31 templates ranging from elliptical to starburst. The libray includes 3 templates of elliptical galaxies and 7 templates of spiral galaxies generated by Polletta et al. (2007) using the code GRASIL (Silva et al. 1998). For the bluest galaxies, they also add 12 templates of starburst galaxies from Bruzual & Charlot (2003) with ages between 3 to 0.03 Gyr. They interpolated between the Polletta template to have a better sampling of the redshift-color space as shown in Ilbert et al. (2009). For the intermediate and late type population, we apply various extinction laws such as Calzetti and Prevot extinction laws (Calzetti et al. 2000; Prevot et al. 1984) with the extinction values E(B-V)=0.1,0.2,0.3,0.4,0.5 as used for the COSMOS survey (Ilbert et al. 2009). Le Phare do not allow combination of templates and create a new template by extinction values. We add emission line fluxes in the magnitude derived for the template library to better reproduce the colors observed in galaxies having strong star-forming region such as starburst.

3.2. BPZ

BPZ is a bayesian photometric redshift estimation based on a template fitting method. They use different sets of priors based on redshift and magnitude distribution from existing surveys. The library is composed by 8 templates PEGASE and 3 starbursts but the code allow combination of several templates in the χ^2 minimisation.

3.3. Definition of photoz quality

To assess the quality of the photometric redshifts for the CLASH data, we compute photometric redshifts of galaxies that have spectroscopic redshifts. We then compute the scatter, the mean and number of outliers of the $photoz - specz$ distribution. The scatter is defined as the robust estimator Normalised Median Absolute Deviation (NMAD) described in Hoaglin et al. (1983) and is $1.48 * |z_p - z_s|/(1+z_s)$, where z_p is the abbreviation for photometric redshift and z_s for spectroscopic redshift. The mean (μ) is the mean value of $z_p - z_s$ and the number of outliers (η) is defined as galaxies whose $|z_p - z_s|/(1+z_s) > 0.15$.

[1] www.cfht.hawaii.edu/ arnouts/lephare.html

3.4. Template representativity

One of main source of systematic errors come from the reliability of the template library in the color space. BPZ and Le Phare redshift estimation is based on a pure χ^2 minimisation with and without the help of sets of priors and template combination such as the BPZ method is proposing. We thus need to check the representativity of our template libraries with the CLASH data using the spectroscopic redshift available.

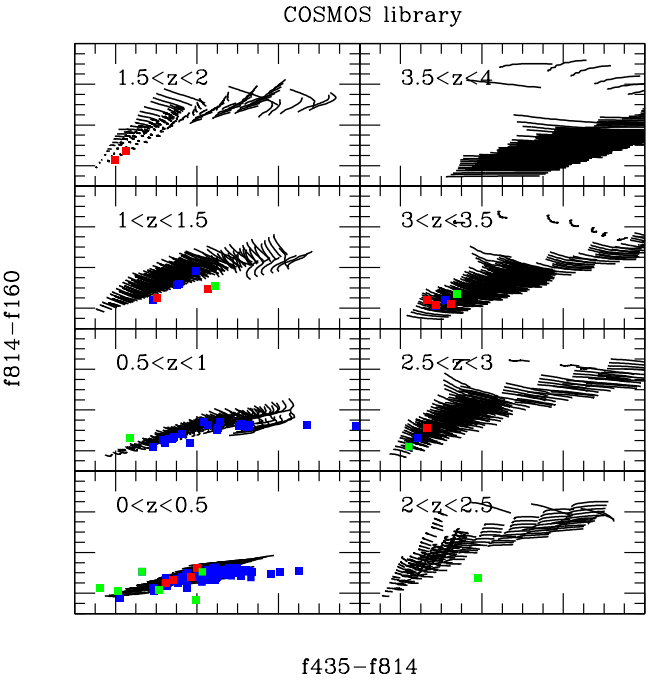

Fig. 2. Colors of the photoz template library for different redshift ranges. The black lines are F435-F814 as a function of F814-F160 of the COSMOS library and the blue, green and red dots correspond to the CLASH observations of the spectroscopic redshift sample. The green and red points correspond to catastrophic redshift for which the odds are respectively lower and higher than 90%

Figure 2 shows the color F435-F814 as a function of the color F814-F160 for different redshifts ranges. The COSMOS library is represented by the black lines, the blue dots are the CLASH observations of the spectroscopic redshifts sample. We show the catastrophic redshifts in red and green. The green points are the "known" catastrophic redshift with odds<90% and the red points are the catastrophic redshift that have a good fit with odds>90%. Our spectroscopic redshift sample contains mainly cluster galaxies at z<1. The strongest color gradient will be from the Balmer/D4000 breaks in the F435-F814. The photoz accuracy will mainly rely on the library colors of the Balmer/D4000 breaks at different redshift. The COSMOS template colors show a good agreement with the CLASH specz sample. To quatify this, we perform a Kolmogorov-Smirnov test.

TODO : Kolmogorov-Smirnov test

We note than some of the CLASH observations colors are not represented in the library. In those case, the odds value decrease and indicate that the redshift is likely misestimated as shown by the green points.

TODO : Need to investigate the red points...

4. CLASH photometric redshift accuracy

Using Le Phare and BPZ described in section 3, we compute photometric redshifts for all clusters of the CLASH survey. In this section, we first study the photoz quality using the spectroscopic redshift of galaxies at $z < 1$.

4.1. Photometric redshift and systematics from the photometry

We compute photometric redshift using different subset of the CLASH filters. In order to show the utility of all filters, we compute photoz for 6 subsamples of filters :

- optical filters of the ACS camera
- NUV+optical filters of the WFC3/UVIS+ACS cameras
- ACS+NIR filters of the ACS+WFC3/IR camera
- UVIS1(F390W)+ACS+NIR of ACS+WFC3
- UVIS2(F336W+F390W)+ACS+NIR of ACS+WFC3
- NUV+optical+NIR filters of ACS+WFC3 (all CLASH photometry)

These tests allow to check possible bias in the photometry that could be related to the camera.

The galaxies for which we have a spectroscopic redshift are bright galaxies of the cluster field with a S/N>10, except for the arcs candidates. These galaxies have an accurate photometric redshift estimation with very peaked p(z). Without any selection and using all bands, we reach an accuracy of 3.5%(1+z). Table 2 gives the photoz accuracy for a subset of the specz sample. The UVIS2+ACS+NIR is the best configuration for our spectroscopic redshift sample since we are looking at galaxies at z<1 for which the Balmer/D4000 breaks are in F390W and F435W. Discarding the 2 bluest filter avoid possible biais when computing the systematic shifts with cosmic-rays contamination from the UVIS photometry. However, the bluest filters help the photometric redshift estimation for galaxies at z>2 typically the arcs as shown in 5.

Table 2. Quality of the photometric redshift compared to spectroscopic redshifts for all CLASH cluster. In this table, we select galaxies with a S/N>10 in F814 with an odds cut at 99% and for which $z_s < 1$ up to F814 26 AB magnitude. The first column is the subset of filters in which we compute photoz, the second and third column are the NMAD and the mean of the $z_p z_s$ distribution. The 2 last columns are the fraction of the specz sample and the number of catastrophic redshift.

Photometry	NMAD	$\mu[\Delta z/(1+zs)]$	% gal	η
"ACS"	0.04101	-0.01935	40.4	1
"UVIS_ACS"	0.03419	-0.008538	27.1	2
"ACS_NIR"	0.03151	-0.01055	66.3	1
"UVIS1_ACS_NIR"	0.02748	-0.01173	73.5	1
"UVIS2_ACS_NIR"	0.02695	-0.005607	69.3	3
"UVIS_ACS_NIR"	0.03107	-0.006041	70.5	4

TODO : Need to add BPZ results

These results include systematic shifts in the photometry computed using the spectroscopic redshift sample. The shifts values are shown in Table B.1. These shifts accounts for possible biases in the photometry together with differences between the CLASH colors and the library colors. We find shifts that are not higher than 0.3 showing a relatively good agreement between observations and models.

Both the BPZ and Le Phare show good photoz estimations for the CLASH observations. The systematic shifts applied to the photometry have been computed using the whole spectroscopic redshift sample.

Figure 3 show the photometric redshift as a function of spectroscopic redshift for the specz sample. The red points are the galaxies with a S/N>10 and odds¿97%. This represent 76% of the CLASH specz sample for which we reach an accuracy of 0.033%(1+z) using all bands.

TODO : Need to study the catastrophics in looking at their SED fits and photometry

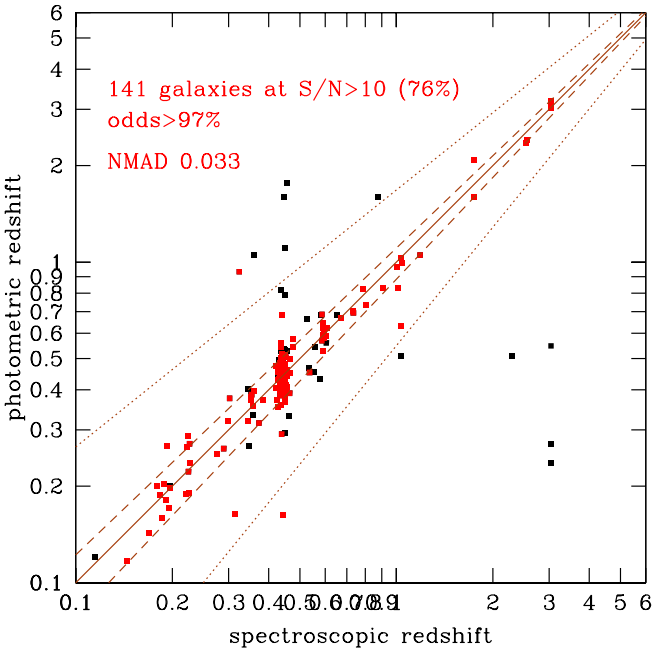

Fig. 3. Spectroscopic vs photometric redshift for all CLASH clusters. The red points correspond at galaxies with odds¿97% and the black points without any selection. The brown dashed, and dotted curves correspond to respectively at $z_p = z_s \pm 0.02(1+z_s)$, and $z_p = z_s \pm 0.15(1+z_s)$.

In order to study the reliability of the photometric redshift estimation, we look at the 1- and 2-σ confidence region. Figure 4 shows the cumulated distribution of $[z_p - z_s]/(1,2) - \sigma$ diagram. This figure show that about 60% of the photoz falls into the 1-σ region and about 92% falls into the 2-σ regions. This results shows that our photoz estimations are statistically consistent.

4.2. Photometric redshift on simulated CLASH photometry

Using the simulations of Jouvel et al. (2009), we simulated the photometry of the CLASH observations. We aim at testing the capabilities of the CLASH photometry at estimating a photometric redshift. We also show the limitations of broad-band photometry. We use catalogues coming from Le Phare simulations with templates from Coleman et al. (1980) extended in wavelength with synthetic spectra from Bruzual & Charlot (2003). There is 5 main template and 1 starburst one that are interpolated linearly in 66. The luminosity function comes from Dahlen et al. (2005) and has been adapted to fit the COSMOS observations as explained is Jouvel et al. (2009). The depth in each band is calculated to match the CLASH survey depth shown in Table 1.

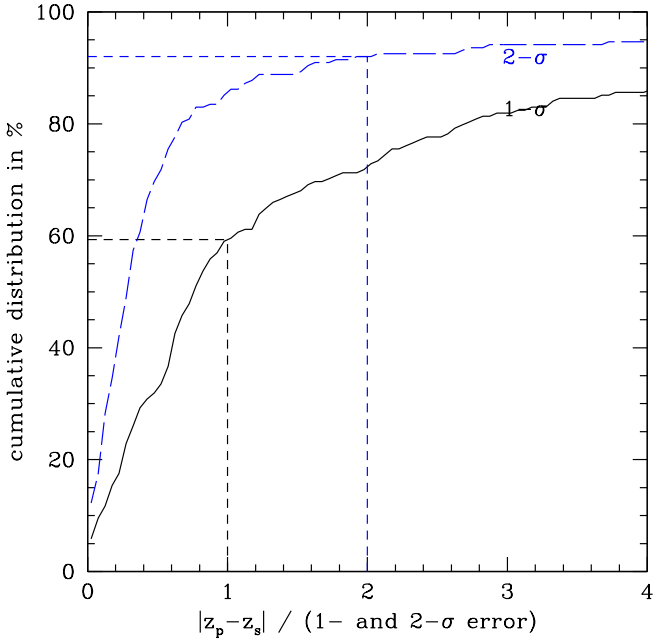

Fig. 4. Cumulated distribution of $[z_p - z_s]/(1,2) - \sigma$ for all CLASH clusters.

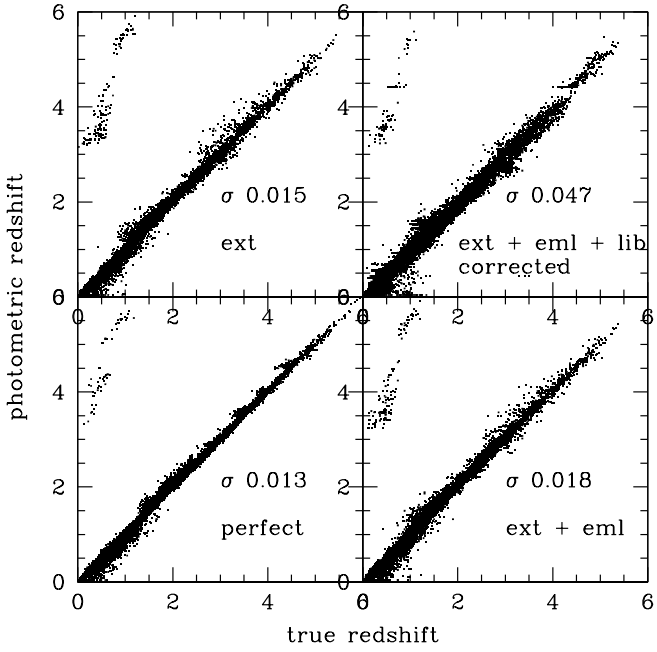

Fig. 6. Photometric redshift results for simulations of the CLASH data using the depth listed in Table 1.

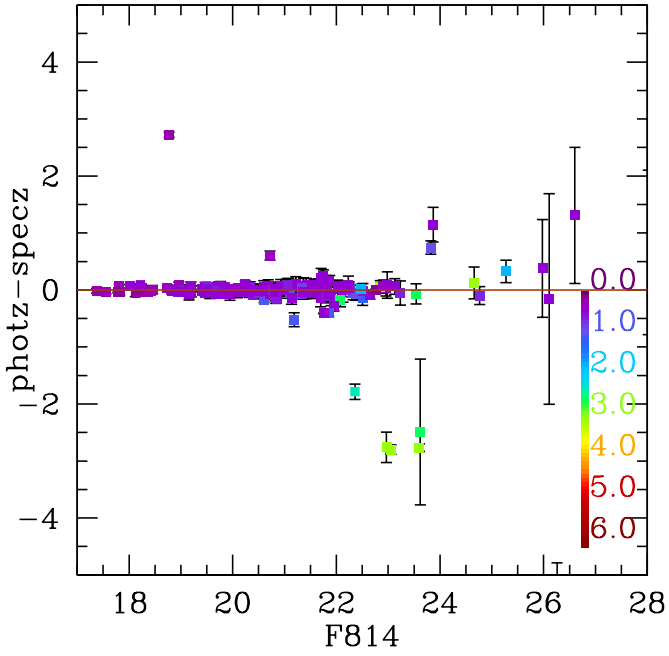

Fig. 5.

We use Le Phare simulation and made 4 different catalogues of increasing complexity.

Figure 6 shows the photometric results of these 4 catalogues. The scatter quoted in the different panels is the NMAD as explained in section 3.3. The bottom left panel is the perfect case for which the templates are the same to derive the magnitudes in the CLASH bands and to estimate the photometric redshifts. The top left panel represents the photometric redshift when we add extinction to the template set for both the mock photometry and the photoz library. The bottom right panel, we include both extinction laws and emission line fluxes in the mock galaxies and in the photoz library. Then, in the top right panel, we keep the same level of complexity than for the bottom right panel but we do not use the same template to generate the mock galaxies and for the photoz library. This last change increase the scatter by 2.6 times. In the best case, if the colors of our library is representative of the observation, we should be in case 3 with a scatter of 0.018. We should then be able to reach in the best case close to 0.02*(1+z).

5. Photometric redshift of MACS1206 multiple images systems - Arcs

MACS1206 cluster has first been observed by the Massive Cluster Survey (MACS) described in Ebeling et al. (2001). This cluster has a strong flux in X-ray and shows a smoothed relaxed profile which are 2 of the criteria in the MACS survey selection function (Ebeling et al. 2001). The first mass model of this cluster has been derived from the F814W/HST imaging using one giant arc as described in Ebeling et al. (2009). This cluster has been recently observed by the CLASH program in 16 bands allowing the discovery of 47 new multiple images of 12 sources for which 4 of them have a spectroscopic redshift as described in Zitrin et al. (2011). One multiple image system is at redshift z=1.033 and is described in Ebeling et al. (2009). The others systems have been observed by the VIMOS/VLT instrument as part of VLT/VIMOS Large Programme 186.A-0798 which will target 14 southern CLASH clusters. The other systems are at redshift 2.54 and 3.03.

We have four systems of arcs for which we have spectroscopic redshift from Ebeling et al. (2009). To assess the accuracy of our photometric redshift for the strong lensing, we ran our photoz codes on these systems. Below, we detail each systems and present photometric redshifts from Le Phare and BPZ and also show a photometric redshift for a combination of the arcs in each system.

Indeed, a system of arcs has supposedly the same object source lensed by MACS1206 in this paper. It is then possible to recover some informations about the source in doing combined analysis of the photometry for all the arcs in supposing the identification is valid. However, the level of systematic uncertainties is quite high. A first systematic error comes from the structures along the line of sight. The light for each of the multiple images followed a different path to the cluster, there is then possible contamination by structures along the line of sight. A second one comes from Then each of the multiple images may have a slightly different spectral type due to differential magnification and photometric contamination. However the redshift for all the images should be equal. The procedure would be to marginalize over templates before multiplying the probabilities. We then can multiply the p(z) for each arc because the measurements are independent, in the statistical sense except for any systematics which affect all our observations equally.

An other procedure consist in multiplying for each arc the full redshift-template χ^2 values and then marginalize over the templates to have the combined p(z). In this paper, we implement both method and show results for the four systems below.

5.1. System 1

System one has three arcs from a source galaxy at redshift 1.033 for which spectroscopy has been obtained by Ebeling et al. (2009). We have good photometry for all the arcs in 15 filters for images 1.1 and 1.2 and 14 filters in 1.3 where we miss the F435 filter as you can see in figure 7. Figure 7 show the CLASH observations in square points for the different multiple images and their best-fit spectra from the Le Phare. Multiple image 1.1 is in green dashed lines, 1.2 in red dotted lines and 1.31.31.3blue solid lines. The best-fit redshift and templates are given in Table 3. Table 3 gives in column order, the arc identifiant, the best redshift and 95% confidence region from Le Phare, the χ^2 value for Le Phare best-fit, the best-fit redshift from Le Phare after marginalisation over the templates, the best-fit redshift from BPZ, the best-fit template and odds from Le Phare and the number of filter used for the fit.

We derived photometric redshift with and without the zeropoint corrections calculated in **??**. We show in figures and tables the results without zeropoint correction by default since the zeropoint correction might not be very reliable as explained is **??** When the difference is significant (more than 2σ), we show both results and add to the arc id a small "s" for the zeropoint-shifted photometry one.

For system one, the three multiple images have close best-fits except for arc 1.1. For this arc, the systematic shift of the photometry seems to help the fit and give a photometric redshift closer to the spectroscopic redshift. Arcs 1.2 and 1.3 are within 2-sigma from the true redshift for BPZ and Le Phare results. All best-fits are starbursts galaxies. The arcs 1.3 has a high odds and a good χ^2 value, it is the closest fit to the spectroscopic redshift.

Figure 7 shows the marginalized redshift probability of each arcs in solid blue lines. The dot-dashed black line is a combination of the three multiple images made from the multiplication of the marginalized over template redsfhit probability p(z) of each arc. The dahsed red curve is a combination of the three multiple images that we obtain in multiplying the probabilities of redshift-template p(z,T) for the three arcs and then marginalizing over templates to give a redshift probability. As you can see in Figure 7, this last solution shows a closer solution to the spectroscopic redshift. We apply a flat prior over template and redshift in this procedure.

Table 3. Photometric redshift for system 1 of MACS1206. The spectroscopic redshift for this system is 1.033.

Arc	z^{lp}_{best}	χ^2_{best}	z^{lp}_{marg}	z^{bpz}_{best}	mod	odds	#
1.1	$0.852^{+0.014}_{-0.014}$	162		-	29	99	15
1.1_s	$1.051^{0.000}_{-0.014}$	190		-	28	100	15
1.2	$1.065^{+0.022}_{-0.027}$	195		$1.04^{+0.08}_{-0.08}$	29	100	15
1.2_s	$1.103^{0.018}_{0.001}$	178		$1.04^{+0.08}_{-0.08}$	30	100	15
1.3	$1.052^{+0.025}_{-0.021}$	12		$1.01^{+0.08}_{-0.08}$	28	100	14
1.3_s	$1.116^{0.012}_{-0.007}$	48		$1.01^{+0.08}_{-0.08}$	24	100	14

5.2. System 2

System two has three arcs from a source galaxy at redshift 3.03 for which spectroscopy has been obtained by Ebeling et al. (2009). We have good photometry in the visible and NIR for all the arcs 12 filters. For the filters of the UVIS camera, the photometry is less accurate. We do not correct for cosmic rays in the UVIS filters, this can be a source of systematic errors in the photometry measurement. Figure 7 show the CLASH observations and best-fit spectra for the multiple images. The symbolism is the same as for figure 7 for system 1. The best-fit redshift and templates are given in Table 4. Table 4 has the same format as Table 3.

The arc 2.1 has a bad fit with a very high χ^2 value probably caused by the uncertain photometry in both the UVIS and the bluest visible bands. We think it probably comes from contamination by the cluster light or structure along the line of sight. **can we check the photometry for this arc? and the aperture size?** We note arc 2.2 has the best χ^2 and odds value and is the closest to the spectroscopic redshift.

Figure 7 shows the marginalized redshift probability for system 2. The symbolism is the same as in Figure 7. We note that the marginalized and combined p(z) are closer to the spectroscopic redshift than the best-fit redshift only as it was the case for system 1.

Table 4. Photometric redshift for system 2 of MACS1206. The spectroscopic redshift for this system is 3.03.

Arc	z^{lp}_{best}	χ^2_{best}	z^{lp}_{marg}	z^{bpz}_{best}	mod	odds	#
2.1	$3.207^{+0.051}_{-0.071}$	473		-	31	99	14
2.1_s	$3.134^{0.099}_{-0.058}$	474		-	30	100	14
2.2	$3.195^{+0.204}_{-0.092}$	15		$3.4^{+0.17}_{-0.17}$	31	99	15
2.2_s	$3.119^{0.095}_{-0.089}$	25		$3.4^{+0.17}_{-0.17}$	30	99	15
2.3	$3.642^{+0.081}_{-0.063}$	28		$3.68^{+0.18}_{-0.18}$	24	99	15
2.3_s	$3.194^{0.078}_{-0.094}$	37		$3.68^{+0.18}_{-0.18}$	30	97	15

5.3. System 3

System three has three arcs from a source galaxy at redshift 3.03 for which spectroscopy has been obtained by Ebeling et al. (2009). As for system 2, the photometry is not very good in the UVIS filter which do not help the fitting procedure. Figure 7 show the CLASH observations and best-fit spectra for the multiple images. The best-fit redshift and templates are given in Table 5. Table 5 has the same format as Table 3 and 4. Arcs 3.1 and 3.3 have very similar photometry except in the two bluest fil-

ters. They show similar photometric redshift fit as you can see in Figure 7 and Table 5.

For the arc 3.2, there is a big difference in the photometric redshift when comparing with and without zeropoint correction. The zeropoint correction do not help for this arc and this is reflected in the odds value of 43 with zeropoint correction and 90 without. However, it shows better result for the arc 3.3.

Table 5. Photometric redshift for system 3 of MACS1206. The spectroscopic redshift for this system is 3.03.

Arc	z^{lp}_{best}	χ^2_{best}	z^{lp}_{marg}	z^{bpz}_{best}	mod	odds	#
3.1	$3.650^{+0.088}_{-0.063}$	45		$3.73^{+0.19}_{-0.18}$	22	99	15
3.1_s	$3.149^{0.097}_{-0.100}$	45		$3.73^{+0.19}_{-0.18}$	29	97	15
3.2	$2.615^{+0.473}_{-0.134}$	47		-	31	90	14
3.2_s	$1.539^{0.447}_{-0.383}$	40		-	31	43	14
3.3	$3.622^{+0.06}_{-0.117}$	35		$3.52^{+0.18}_{-0.18}$	22	95	15
3.3_s	$3.090^{0.098}_{-0.137}$	43		$3.52^{+0.18}_{-0.18}$	29	93	15

As for systems one and two, the combined and marginalised p(z) gives good result.

5.4. System 4

System four has five arcs from a source galaxy at redshift 2.54 for which spectroscopy has been obtained by Ebeling et al. (2009). As for systems two and three, the UVIS photometry is not very good. Figure 7 shows the CLASH observations and best-fit spectra for the multiple images. The best-fit redshift and templates are given in Table 5. Table 5 has the same format as Table 3 and 4.

Concerning arc 4.4, we think the photometry is contaminated by the cluster light since it is located very close to the BCG. We tried with and without zeropoints and bluest filters, and the photometric redshift was in all cases of $0.520^{0.005}_{0.000}$. For the other arcs photometric redshift are close to the spectroscopic redshift.

Table 6. Photometric redshift for system 4 of MACS1206. The spectroscopic redshift for this system is 2.54.

Arc	z^{lp}_{best}	χ^2_{best}	z^{lp}_{marg}	z^{bpz}_{best}	mod	odds	#
4.1	$2.541^{+0.071}_{-0.075}$	15		$2.99^{+0.16}_{-0.16}$	30	100	15
4.1_s	$2.192^{0.016}_{-0.010}$	40		$2.99^{+0.16}_{-0.16}$	30	98	15
4.2	$2.350^{+0.327}_{-0.186}$	98		$2.54^{+0.17}_{-0.18}$	31	72	15
4.2_s	$2.200^{0.269}_{-0.080}$	102		$2.54^{+0.17}_{-0.18}$	28	73	15
4.3	$1.928^{+0.294}_{-0.024}$	98		$2.35^{+0.19}_{-0.19}$	31	61	14
4.3_s	$2.159^{0.125}_{-0.239}$	109		$2.35^{+0.19}_{-0.19}$	24	92	14
4.4	$0.520^{0.005}_{0.000}$	73		-	13	100	14
4.5	$2.666^{+0.602}_{-0.213}$	7		$3.04^{+0.16}_{-0.19}$	30	65	14
4.5_s	$2.398^{0.323}_{-0.180}$	5		$3.04^{+0.16}_{-0.19}$	29	75	14

For all the systems, BPZ and Le Phare show very close results for most cases at 2σ for one another. We also show that the combination and marginalisation over templates of the multiple images gives a good estimation source redshift. If one want to work with best-fit only, then a combination of high odds and good χ^2 is a good criterion to estimate the photometric redshift validity.

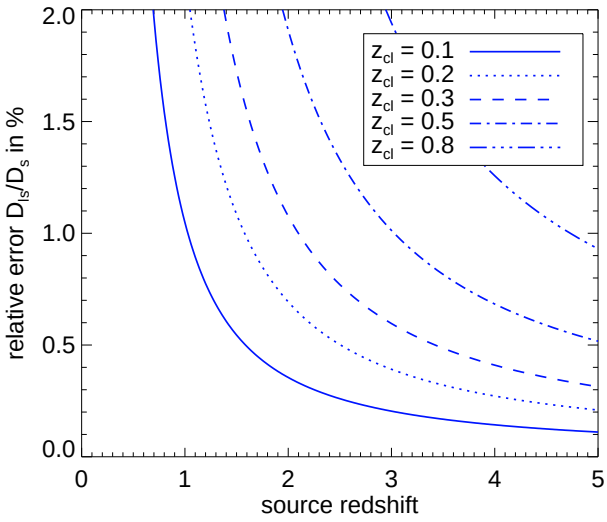

Fig. 8. The relative error on the distance ratio D_{ls}/D_s as a function of source redshift z_s for various lens redshifts z_{cl}, assuming a photoz accuracy of 4%

6. Sensibility of the mass reconstruction from SL to the photoz accuracy

Now we consider the impact of the photoz uncertainty on the lens modeling. The accuracy of the photozs measured for arcs and multiple images directly influences the accuracy of the mass model through the lens equation, which connects the unknown source position β with the image position θ

$$\beta = \theta - \frac{D_{ls}}{D_s}\hat{\alpha}(\theta). \quad (2)$$

The mass model determines the deflection field $\hat{\alpha}$ and the photoz enters in the distance ratio D_{ls}/D_s. Figure 8 shows how the relative photo-z accuracy is mapped to the distance ratio using standard linear error propagation. It is clear that low redshift sources are the most challenging. The relative accuracy of the distance ratio can be regarded as the relative error on the overall mass scale of the lens since $\hat{\alpha} \propto M$ so, e.g., a z=2 source lensed by a z=0.3 cluster will give rise to a relative uncertainty on D_{ls}/D_s and on the total mass of $\sim$1% if the photoz uncertainty is 4%. However, the exact influence of the photoz accuracy on the lens model will depend on the number, positions, and redshifts of the multiple images in a complex way, and it may also depend on whether the lens model is parametric or not. This will be assessed on a case–by–case basis.

However, we can also regard the photo-z uncertainty as a positional uncertainty in the image plane, $\delta\alpha_z$, through the lens equation. The relative accuracy of the distance ratio in Figure 8 is then equal to the relative accuracy on the distance between the image and the model-predicted source position. This approach facilitates comparison with other positional uncertainties that affect the lensing analysis. To be specific, we base our comparison on the 168 multiple images produced by Abell 1689 and their corresponding source positions as found using the lens model of Coe et al. (2010). We imagine that each image has a photometric redshift and that the overall photo-z accuracy is 4%. The disttribution of the photoz positional uncertainties, which we label $\delta\alpha_z$ are shown in Figure 9. We take this distribution as a reasonable sample estimate of the impact of photoz accuracy.

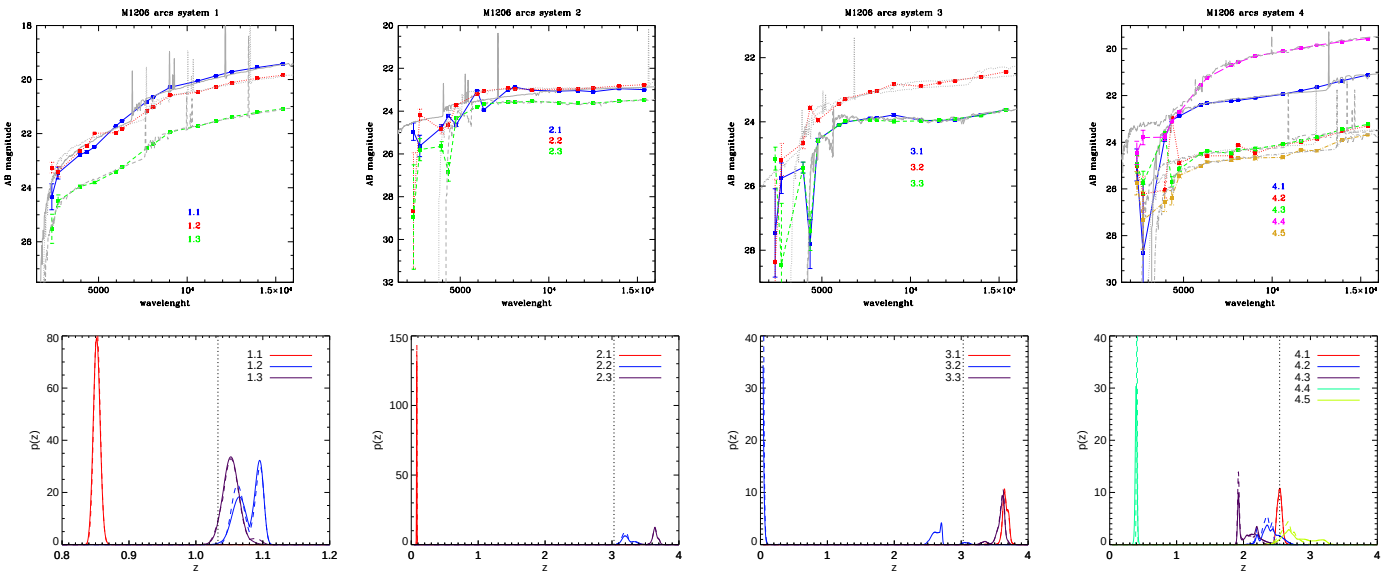

Fig. 7. Spectra of the best-fit template and redshift from Le Phare for system 4 of MACS1206. Marginalized P(z) of Le Phare photometric redshift for system 4 of MACS1206. The solid blue lines are the marginalized p(z) for the different arcs. The black and red dotted lines are a combination and marginalization of the differents arcs.

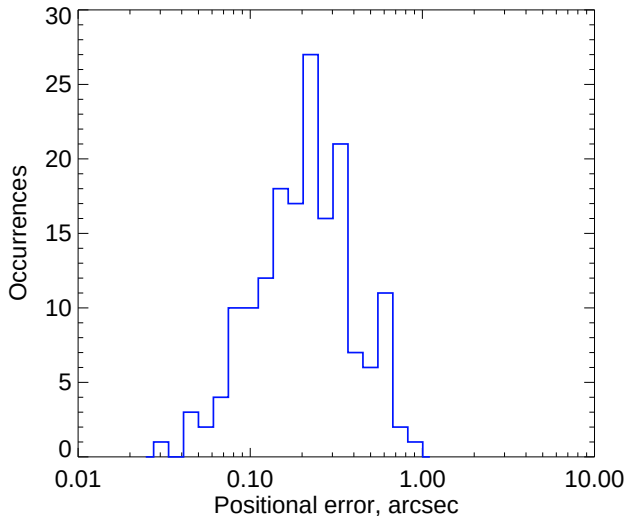

Fig. 9. The distribution of photoz positional errors for the 168 images lensed by Abell 1689.

For *HST* imaging, the accuracy of the astrometric solution is similar to the pixel scale, 0.13 arcsec (CORRECT? REF?). It is clear from Figure 9 that a 4% photoz accuracy implies that, for most images, $\delta\alpha_z$ will be larger than the astrometric error. However, larger positional errors are predicted: Jullo et al. (2010) estimated that images would pick up additional deflections of more than 1 arcsec from lensing by the large-scale structure along the line-of-sight, and it is clear from Figure 9 that we expect almost all $\delta\alpha_z$ to be smaller than this. In a more detailed matter power spectrum analysis, Host (2011) showed that the impact of large-scale structure increases with redshift and distance on the sky to the cluster centre, which means that low-redshift arcs will be relatively more affected by the photo-z accuracy. We calculate the deflection $\delta\alpha_{\rm LSS}$ using the prescription of Host (2011), and we find that $\delta\alpha_z > \delta\alpha_{\rm LSS}$ for 6% of the Abell 1689 images if the photoz accuracy is 4% while this happens for only one image if the accuracy is 2%. Hence, we conclude that the impact of the photoz accuracy of the mass model is most likely subdominant in comparison to the uncertainty associated with lensing by large-scale structure along the line of sight if we can achieve a photoz accuracy of 4% or better.

Finally, there is the possibilty of catastrophic errors arising from the Lyman-Balmer break degeneracy, which can give rise to two solutions in the photoz fitting. However, this is usually a benign case for the purpose fitting the lens model. It is extremely unlikely that the low-*z* solution is a viable redshift for a lensed image, in fact, for *CLASH* clusters, it may well be a lower redshift than the cluster lens itself. Even if the low redshift solution is viable for an arc it will be difficult to fit the observed image positions since the separation between the multiple images would not accommodate the low predicted D_{ls}/D_s – as long as there are other multiple images constraining the mass model. Hence, catastrophic redshifts will mostly be an issue for the identification of multiple images in the first place, and in that case there are other constraints such as morphology which can be used.

7. MACS1206 photometric redshift catalogue

With this paper, we release a photometric redshift catalogue of MACS1206. This catalogue includes the photometry information for each object that has been derived as described in section 2 along with photometric redshift from Le Phare and BPZ.

7.1. The photometric redshift catalogue

We have a total of 2202 objects in MACS1206 catalogue for an area of 4.08 arcmin^2 covered by the whole CLASH filter set as explained in Postman et al. (2012). We give the coordinates of each objects along with some SExtractor output such as an estimation of the size with the full-width-half-maximum, the area used to derive the photometry, an estimation of the ellipticity calculated from the second moment of the light distribution as explained in Bertin & Arnouts (1996) and a probability of the object being a star called stellarity from a neural

network approach. We give the photometry in all CLASH bands to the depth listed in Table 1 and upper-limits when the galaxy is not detected. Concerning the photometric redshift result, we give the best-fit redshift with the 68 and 95% confidence interval redshift for both BPZ and Le Phare. We also add an estimation of the confidence on the photoz called odds for BPZ and PDZ_BEST for Le Phare. This parameter gives the result of the integral of the redshift probability centered at the best-fit redshift with a window width of 2.5 times the photoz accuracy expected for the CLASH survey 0.05. Figure 10 compares BPZ

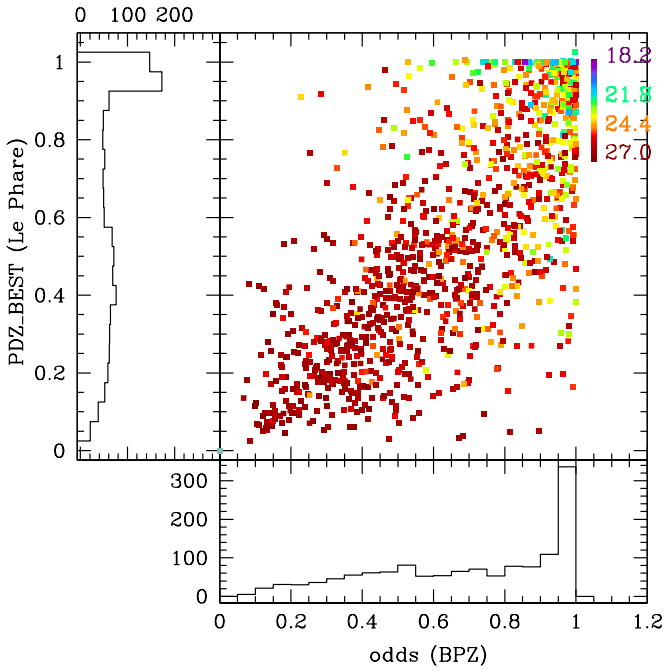

Fig. 10. Comparison between Le Phare and BPZ quality parameter "PDZ_BEST" and "odds" as a function of magnitude for the colors.

odds and PDZ_BEST from Le Phare The color density represents the AB magnitude in the F814W filter. Higher are the odds values and narrower is the peak of the best-fit which usually indicates a good fit and an accurate photoz measurement. Galaxies at low magnitudes have high odds as one could expect. Indeed, low magnitude galaxies have an higher accuracy on the photometry which makes the template-fitting better and in most case a more accurate redshift. Indeed the library we use to derive photoz measurement is representative enough of the color found in the CLASH survey which will give a secure photoz measurement. Le Phare and BPZ agree quite well and find high odds and BPZ_BEST for low magnitude galaxies and low odds and BPZ_BEST at high magnitudes. We also show histograms of the odds and PDZ_BEST which show that most galaxies have a secure measurement of the photoz.

7.2. Finding the cluster redshift

Figure 11 shows photoz histograms at photoz<1 of Le Phare in black solid line and BPZ in blue dashed line. The cyan solid curve represent the redshift of the cluster MACS1206. BPZ and Le Phare curve has been computed using values of odds and PDZ_BEST>0.5. At PDZ_BEST>0.3, we can already detect the cluster and the photoz peak become more accurately defined as we cut at higher values of odds and PDZ_BEST.

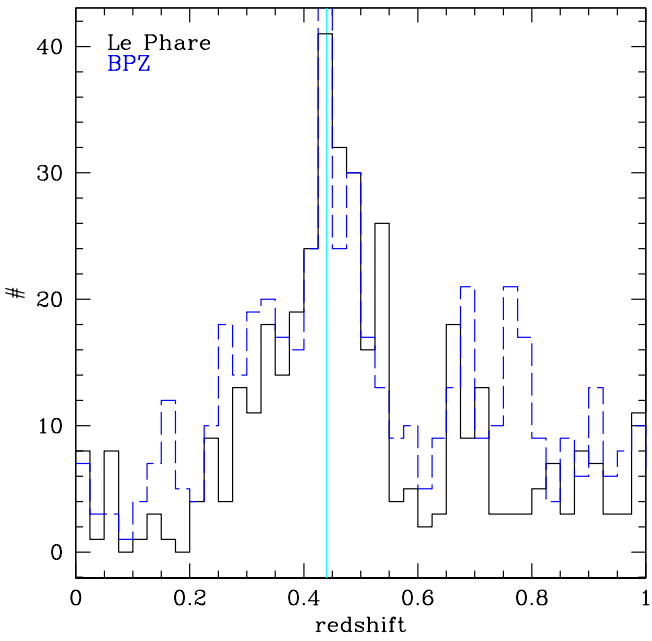

Fig. 11. Photometric redshift histogram of MACS1206 using BPZ in blue dashed line and Le Phare in black solid line.

We note that the fact we are able to detect the cluster redshift shows the reliability of both our photoz.

7.3. Galaxies at z>3

7.4. Mean redshift as a function of radius from the center

Figure 12 shows the mean photometric redshift of galaxies located behind MACS1206 in solid red line as a function of radius from the center of the cluster. The light and dark grey area are respectively the 68% and 95% interval confidence in the photometric redshift around the best fit value. It shows a mean redshift around 1.5 which do not change much as we go further from the cluster center. The mean redshift value is due to the depth of the CLASH observation and shows where most of the weak-lensing signal comes from. It shows that the 68% interval confidence is quite narrow allowing an redshift measurement accurate enough for the weak-lensing analysis. A finner binning in radius also increases the precision of the mean redshift estimate. For the precision estimates of the WL analysis we have to keep in mind that not every galaxy in a photometric/spectroscopic catalogue which is in a redshift intervall under consideration will enter the weak lensing catalogue, because the S/N of galaxies for shape analysis has to be higher than for photometry and because of galaxies have to be significantly extended to measure a shape.

8. Conclusion

Acknowledgements. Stéphanie Jouvel thanks STFC for her postdoctoral support.

References

Benítez, N. 2000, ApJ, 536, 571
Bertin, E. & Arnouts, S. 1996, A&AS, 117, 393
Bruzual, G. & Charlot, S. 2003, MNRAS, 344, 1000

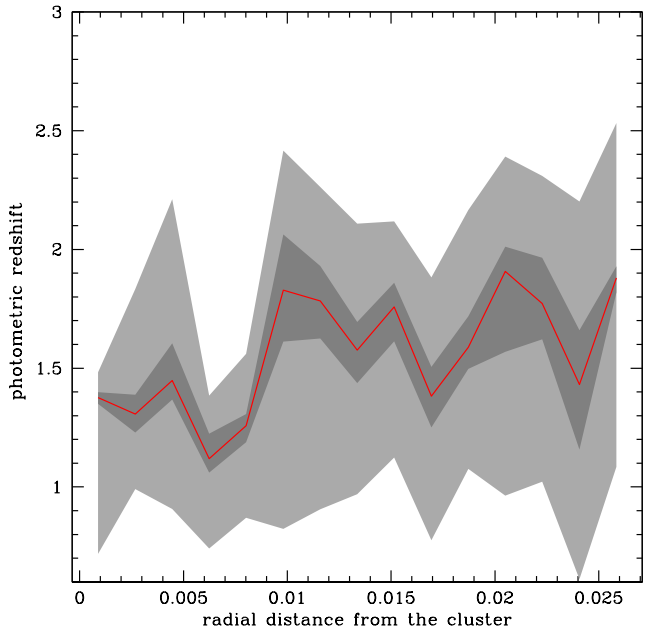

Fig. 12. Mean photometric redshift of galaxies located behind MACS1206 in solid red line as a function of radial distance from the cluster center. The dark grey area reprensent the mean 68% area around the mean and the light grey the 95% area.

Calzetti, D., Armus, L., Bohlin, R. C., et al. 2000, ApJ, 533, 682
Coe, D., Benítez, N., Broadhurst, T., & Moustakas, L. A. 2010, ApJ, 723, 1678
Coe, D., Benítez, N., Sánchez, S. F., et al. 2006, AJ, 132, 926
Coleman, G. D., Wu, C.-C., & Weedman, D. W. 1980, ApJS, 43, 393
Collister, A. A. & Lahav, O. 2004, PASP, 116, 345
Cunha, C. E., Huterer, D., Busha, M. T., & Wechsler, R. H. 2011, ArXiv e-prints
Dahlen, T., Mobasher, B., Somerville, R. S., et al. 2005, ApJ, 631, 126
Ebeling, H., Edge, A. C., & Henry, J. P. 2001, ApJ, 553, 668
Ebeling, H., Ma, C. J., Kneib, J.-P., et al. 2009, MNRAS, 395, 1213
Hildebrandt, H., Arnouts, S., Capak, P., et al. 2010, A&A, 523, A31
Hoaglin, D. C., Mosteller, F., & Tukey, J. W. 1983, Understanding robust and exploratory data anlysis, ed. Hoaglin, D. C., Mosteller, F., & Tukey, J. W.
Host, O. 2011, ArXiv e-prints
Ilbert, O., Arnouts, S., McCracken, H. J., et al. 2006, A&A, 457, 841
Ilbert, O., Capak, P., Salvato, M., et al. 2009, ApJ, 690, 1236
Jouvel, S., Kneib, J.-P., Ilbert, O., et al. 2009, A&A, 504, 359
Jouvel, S., Zoubian, J., & Kneib, J.-P. 2010, in prep.
Jullo, E., Natarajan, P., Kneib, J.-P., et al. 2010, Science, 329, 924
Lamareille, F., Contini, T., Le Borgne, J.-F., et al. 2006, A&A, 448, 893
Polletta, M., Tajer, M., Maraschi, L., et al. 2007, ApJ, 663, 81
Postman, M., Coe, D., Benítez, N., et al. 2012, ApJS, 199, 25
Prevot, M. L., Lequeux, J., Prevot, L., Maurice, E., & Rocca-Volmerange, B. 1984, A&A, 132, 389
Schlegel, D. J., Finkbeiner, D. P., & Davis, M. 1998, ApJ, 500, 525
Silva, L., Granato, G. L., Bressan, A., & Danese, L. 1998, ApJ, 509, 103
Vanzella, E., Cristiani, S., Fontana, A., et al. 2004, A&A, 423, 761
Zitrin, A., Broadhurst, T., Coe, D., et al. 2011, ArXiv e-prints

Appendix A: Spectroscopic redshifts

Table A.1. MACS1206 spectroscopic redshift

Flag	#	# in HST area	provenance
1	110	7	VLT less secure (80%)
2	191	5	VLT emission line
3	302	21	VLT ”archival” [2]
4	2	2	VLT/Keck (Lamareille et al. 2006)
5	3	0	Jones04,09 [3]
6	49	28	Ebeling et al. (2009)
7	28	28	GISMO (Dan Kelson et al.)
8	2	0	VLT secure AGN
9	388	19	VLT secure
10	166	13	VLT very secure

Appendix B: Systematic shifts applied to the CLASH observations

Table B.1. Systematic shifts for different filter configurations

Band	ACS	ACS+NIR	UVIS+ACS	UVIS+ACS+NIR	UVIS1+ACS+NIR	UVIS2+ACS+NIR
F225W	-	-	0.07548	0.22628	-	-
F275W	-	-	0.05326	0.20385	-	-
F336W	-	-	-0.24089	0.03816	-	0.00297
F390W	-	-	-0.00714	0.05394	-	0.01934
F435W	-	-	-0.00116	0.03956	-	-0.00885
F555W	-	-	0.01256	0.01457	-	-0.00599
F475W	-	-	0.02051	0.16240	-	0.16167
F606W	-	-	-0.03777	-0.07409	-	-0.06637
F625W	-	-	-0.02725	-0.04412	-	-0.03455
F775W	-	-	-0.00538	-0.03657	-	-0.03067
F814W	-	-	0.01297	-0.01752	-	-0.01695
F850LP	-	-	0.01482	-0.04418	-	-0.04041
F105W	-	-	-	-0.00606	-	0.00052
F110W	-	-	-	-0.00649	-	-0.00395
F125W	-	-	-	0.03380	-	0.03851
F140W	-	-	-	0.03467	-	0.03440
F160W	-	-	-	0.02503	-	0.01972